

Showcasing research from Alexander J. C. Kuehne's Lab at DWI – Leibniz Institute for Interactive Materials in Aachen, Germany

Water-soluble dopamine-based polymers for photoacoustic imaging

Polydopamine can be converted into linear and water-soluble melanin, which is applied as a nature-identical photoacoustic imaging probe. Here, the melanin polymer is excited with a pulsed infrared laser beam leading to the emission of ultrasound waves, therefore facilitating bio-medical imaging through centimeter thick tissue.

As featured in:



See Alexander J. C. Kuehne et al., Chem. Commun., 2015, **51**, 6084.



ChemComm



COMMUNICATION

View Article Online
View Journal | View Issue



Cite this: *Chem. Commun.*, 2015, 51, 6084

Received 3rd January 2015, Accepted 4th February 2015

DOI: 10.1039/c5cc00039d

www.rsc.org/chemcomm

Water-soluble dopamine-based polymers for photoacoustic imaging†

Tatjana Repenko,^a Stanley Fokong,^b Laura De Laporte,^a Dennis Go,^a Fabian Kiessling,^b Twan Lammers^{bc} and Alexander J. C. Kuehne*^a

Here we present a facile synthetic method yielding a linear form of polydopamine *via* Kumada-coupling, which can be converted into water-soluble melanin, generating high contrast in photoacoustic imaging.

Polydopamine and its derivatives constitute a powerful class of materials of high biological relevance with a multitude of applications. 1-3 Synthetic polydopamines are applied as biomimetic (mussel-)adhesives⁴ and in metal-coordinating membranes for water purification.⁵ The oxidized form of polydopamine, melanin, is ubiquitous in almost all living beings in nature as a granular pigment.6 As such, it constitutes an evolutionarily optimized absorber of light, with extremely high photo-stability. Synthetic versions of melanin have been explored as nature-identical absorbers in organic electronics,7 sun-screen,8 and hair-colorants,9 and also to study the mechanism behind the formation of skin cancer. 10 Besides acting as a radical scavenger, melanin reduces UV-induced DNA damage in skin cells due to its broad absorption profile allowing thermal relaxation of the photoexcited state. 11-14 The latter has sparked interest in melanin as an endogenous and nature-identical photoacoustic contrast agent in bio-medical imaging. Synthetic melanin can be prepared in a base-catalyzed oxidation of dopamine or tyrosine in air. 12,15 First, polydopamine is produced, which is then converted into melanin upon further oxidation. 1,16-18 However, when employing this standard synthetic protocol, only ill-defined polymeric network

To polymerize dopamine in a controlled manner, we first brominate using elemental bromine in a mixture of acetic acid and chloroform. The dibrominated product precipitates during synthesis, limiting the amount of unwanted tribrominated byproducts and pushing the reaction equilibrium further towards the product side. We obtain a mixture of *para-* and *meta-*dibrominated dopamine isomers (see Scheme 1). Both monomers will yield a conjugated polymer, however, only the polymer prepared from the *p-*isomer can be further oxidized to melanin. Therefore, we aim for high levels of the *p-*dibromo dopamine. The mixture of dopamine is

structures or particles are obtained, 19 with controversy about the nature of crosslinking. Covalent and several types of supramolecular crosslinking have been reported. 1,16-18,20 Moreover, the resulting melanin polymers are insoluble in water, preventing their stabilization and their potential application in formulations for creams, lotions or imaging agents.7 Recently melanin and other conjugated polymer nanoparticles have been applied as photoacoustic imaging probes.^{21,22} These materials are resistant to biodegradation. Also natural melanin cannot be degraded enzymatically because of its chemically inert nature and its dense and heterogeneous network structure, which limits enzyme accessibility. 23-25 Due to their size of up to several tens of microns, melanin granules cannot be excreted renally, obviating their use as injectable contrast agents. To alleviate these drawbacks and harness the full biomedical potential of melanin, chemical routes for the precise synthesis towards linear polydopamine and noncrosslinked melanin need to be developed. Such materials would constitute nature-identical contrast agents for biomedical imaging and other viable applications in connected fields. Here we attempt to meet these requirements by synthesizing a controlled covalent form of polydopamine via nickel-catalyzed Kumada cross-coupling.²⁶ The hydroxyl and amine groups of dopamine are protected during synthesis to prevent crosslinking (see Scheme 1).²⁷ After polymerization and removal of the protection groups, polydopamine can be oxidized into a linear form of melanin. We monitor this process in solution by optical spectroscopy and showcase the application of these materials as photoacoustic contrast agents, obtaining very good contrast properties and detection depths of more than 10 mm.

^a DWI – Leibniz Institute for Interactive Materials, RWTH Aachen University, Forckenbeckstraße 50, 52074 Aachen, Germany.
E-mail: kuehne@dwi.rwth-aachen.de

b Department of Experimental Molecular Imaging, University Clinic and Helmholtz Institute for Biomedical Engineering, RWTH Aachen University, Pauwelstraße 30, 52074 Aachen. Germany

^c Department of Controlled Drug Delivery, MIRA Institute for Biomedical Technology and Technical Medicine, University of Twente, P. O. Box 217, 7500 AE Enschede, The Netherlands

 $[\]dagger$ Electronic supplementary information (ESI) available: Experimental details on the synthetic procedures, analyses and cytotoxicity test. Fig. S1: GPC and 1 H-NMR analysis, Fig. S2: detection limits and Fig. S3: cell viability and morphology. See DOI: 10.1039/c5cc00039d

Scheme 1 Dopamine is brominated using elemental bromine in acetic acid and chloroform (a). After recrystallization in acetic acid the p-compound can be isolated and protected using tBoc (b). To obtain polydopamine the protected dibromodopamine is subjected to Kumada coupling at 60 °C (c) and then oxidized in aqueous solution using air (d).

purified three times by recrystallization from acetic acid, affording p-dibrominated dopamine in 96% purity with only 4% of residual m-dibrominated dopamine as determined by ¹H-NMR analysis.

To improve solubility in organic solvents and to inhibit crosslinking during polymerization, all functional hydroxyl and amine groups are protected using *Boc (see Scheme 1). The *Boc-protected p-dibrominated dopamine is polymerized in THF by Kumada coupling. The polymer is collected after precipitation and purification by washing with THF and water. The polymerization yields a polydopamine molecular weight of $M_{\rm w}$ = 5900 Da and a polydispersity index D = 1.02, as determined via GPC (see ESI,† Fig. S1a). The narrow D suggests a living polymerization mechanism, which is the case for Kumada coupling.²⁶ The precipitation of the polymer during synthesis might further support low D. We confirm the molecular weight using end-group analysis in ¹H-NMR (see ESI,† Fig. S1b). The molecular weight is sufficiently low to allow for renal excretion of the polymer and therefore potential in vivo application.

The ¹H-NMR spectrum of the synthesized polydopamine reveals that only the amine remains ^tBoc-protected, indicating that the other ^tBoc-residues are removed thermally from the hydroxyl groups during synthesis (see ESI,† Fig. S1b). The mono-*Boc-protected dopamine polymer is soluble in DMSO and DMF. We deprotect the polymer by treating an aqueous dispersion of the protected polydopamine with hydrochloric acid. After deprotection, the polydopamine is soluble in water. We then oxidize polydopamine in solution by exposure to air.28 Upon oxidation, the colorless solution turns brown, indicating the formation of melanin (see insets in Fig. 1a). We monitor the oxidation process by GPC and do not see the formation of larger molecular weight material, confirming the formation of only linear melanin (see ESI,† Fig. S1a). The conversion of polydopamine to melanin can also be monitored by absorption and fluorescence spectroscopy. Upon excitation at 300 nm, polydopamine fluoresces in the UV/blue spectrum, with a maximum at \sim 360 nm (see blue data in Fig. 1a). Polydopamine exhibits a second absorption band

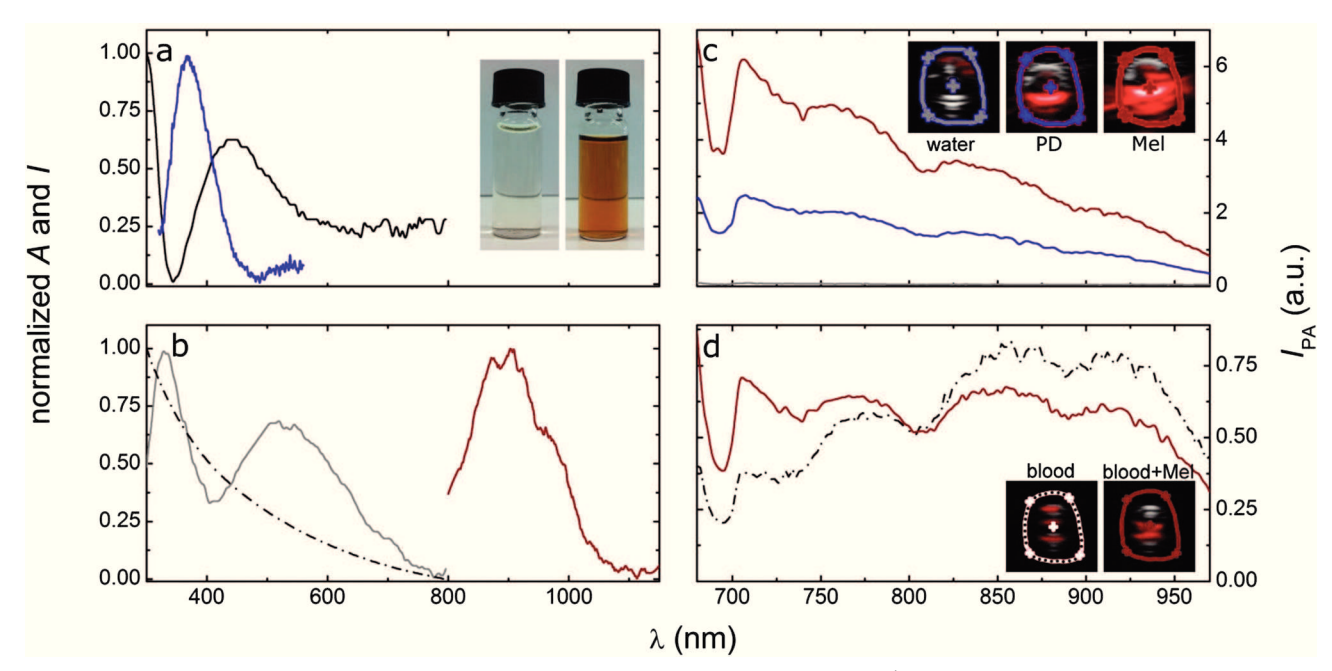


Fig. 1 (a) Absorption (black) and fluorescence (blue) spectra of polydopamine in water ($c = 3 \text{ g L}^{-1}$). (b) Absorption (gray) and NIR fluorescence (red) $(\lambda_{\rm ex} = 785 \text{ nm})$ spectra of melanin in water. The dotted black line represents the absorption profile of natural sepia eumelanin, (c) Photoacoustic excitation spectra of water (gray; largely overlapping with x-axis), polydopamine in water (PD; blue) and aqueous melanin (Mel; red). The insets display the corresponding photoacoustic tomography cross-sections of the phantoms. (d) Photoacoustic excitation spectra of full blood (dotted black) and full blood containing melanin (blood + Mel; red). The insets display the corresponding photoacoustic tomography cross-sections of the blood vessel phantoms.

ChemComm Communication

at ~445 nm, which is broader and lower in absorbance (see black data in Fig. 1a). Upon oxidation of polydopamine to melanin, the absorption bands are bathochromically shifted due to the enlarged π -conjugated system of the polymer (see gray data in Fig. 1b). As a result, the fluorescence is shifted from the UV/blue to the near IR spectrum, as shown in Fig. 1 (red data). The absorption spectrum of the linear melanin converges towards the exponentially decaying absorption profile of commercially available eumelanin (see dotted black curve in Fig. 1b). The broad-band absorption of natural eumelanin is caused by its structural and chemical heterogeneity. The monotonic absorption profile is the result of the superposition of a large number of electronic transitions contributed by different sub-units of natural eumelanin. 23,29 The absorption spectrum of our synthetic melanin does not show this monotonic profile because of its defined and linear structure. The oxidation is controlled so that π -conjugation occurs only along the backbone of the linear polymer. The absorption spectra exhibit two absorption bands: a sharp peak corresponding to the $\pi \to \pi^*$ transition and a broad peak at lower energies corresponding to the $n \to \pi^*$ transition in the conjugated melanin polymer.¹³

For application as a photoacoustic imaging agent, it is important to investigate the properties of the material in the near-infrared (NIR) window, with a spectral range of 650-1300 nm, where biological tissue shows a minimum in absorption. Upon excitation at 785 nm, an aqueous solution of our synthetic melanin shows fluorescence with a maximum at ~ 900 nm (see red spectrum in Fig. 1b). The broad absorption profile, large stokes shift and emission in the NIR spectrum are indicative of the thermoelastic effect needed for photo-acoustic imaging, in which pulsed laser light is transferred into heat fluctuations and eventually into sound waves, which can be detected using an ultrasound transducer. For the characterization of the prepared materials, we prepare 10 mM aqueous solutions of polydopamine and linear melanin, and inject them into blood vessel-mimicking tubes with a volume of $\sim 50 \ \mu L$. These phantom blood vessels are then subjected to

photoacoustic imaging in combination with conventional ultrasound imaging.

The photoacoustic intensity I_{PA} is overlaid with the ultrasound data to obtain a tomographic composite image, displaying the crosssection of the phantom blood vessels (see insets in Fig. 1c). The blood vessel phantoms display high intensity for melanin, a weaker signal for polydopamine, and no signal in the case of water. We also record excitation spectra and obtain the same trend. Melanin gives the best photoacoustic response, with maximum ultrasound emission upon excitation at \sim 700 nm (see red data in Fig. 1c). This excitation maximum is beneficial as blood with (de-)oxygenated hemoglobin has low absorption at this wavelength. This can be exemplified by mixing a 10 mM melanin solution with full blood in a 1:5 ratio, and by comparing the photoacoustic excitation spectrum with the one obtained using melanin-free full blood. The photoacoustic intensity generated at ~700 nm is clearly higher for melanin enriched blood, as shown in Fig. 1d. At higher excitation wavelengths, the pure blood sample exhibits stronger ultrasound emission, while the melanin containing sample has a lower photoacoustic response in this region, reflecting the low photoacoustic efficiency of melanin at wavelengths exceeding ~800 nm (cf. Fig. 1c). We determine the detection limit of the linear melanin and compare it to Aurovist™, which are commercially available gold nanoparticles with a diameter of 1.9 nm.30 The detection limit of the linear melanin exceeds that of the gold nanoparticles by two orders of magnitude (see Fig. S2, ESI†).

Having determined the optimal excitation wavelength and the detection limit in a non-physiological environment, we move on to photoacoustic imaging using biological phantoms. To find a suitable concentration for imaging, we inject 100 µL of solutions containing increasing amounts of melanin subcutaneously into dead mouse phantoms, and analyze the photoacoustic response upon excitation at 706 nm. Already at a melanin amount of 100 nmol, a clear signal is apparent. At 10 nmol of melanin, no discrimination between the sample and the melanin-free control

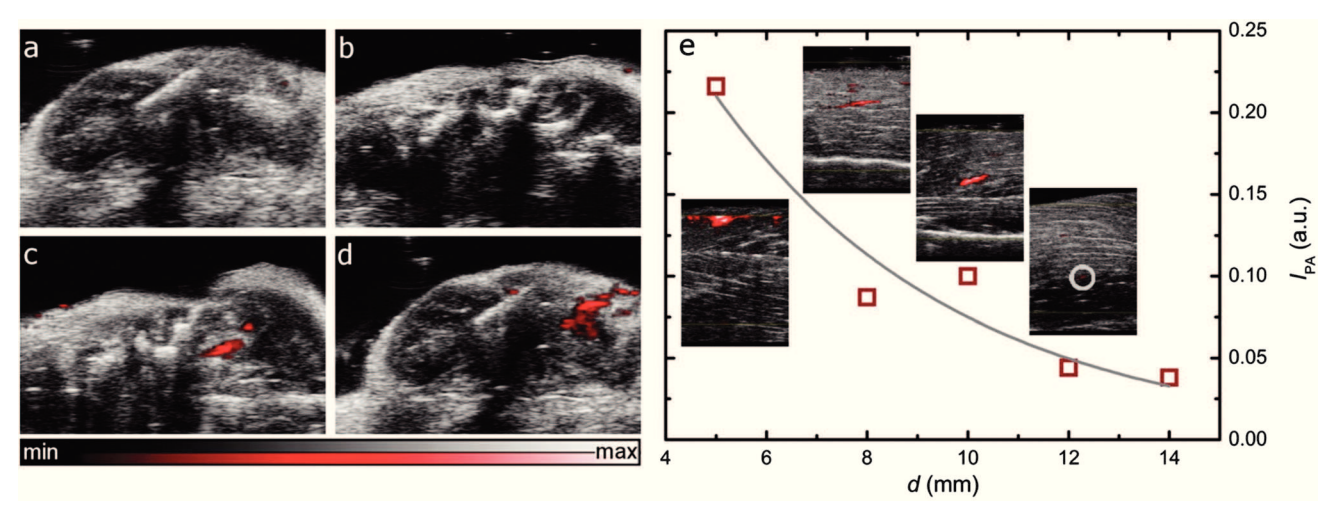


Fig. 2 (a-d) Photoacoustic tomography images of mice subcutaneously injected with 100 µL of aqueous solutions containing (a) no melanin, (b) 10 nmol, (c) 100 nmol and (d) 1 µmol of melanin. (e) Depth-dependence of the photoacoustic signal, analyzed via injecting 100 µL of a 1 mM melanin solution into chicken breast. The insets show the photoacoustic tomography images, clearly displaying the melanin contrast agent in red. The gray circle in the photoacoustic tomogram highlights the melanin signal at a depth of 12 mm, which is just visible

Communication ChemComm

is possible, as shown in Fig. 2a-d. To determine the depthdetection limit, we continue with 100 nmol of melanin in 100 μL aqueous solution, and inject into a chicken breast phantom at increasing depths to record the photoacoustic emission together with the ultrasound reflection. The photoacoustic intensity $I_{\rm PA}$ decreases exponentially with injection depth d, which is typical for biological tissue, as shown in Fig. 2e. Up to a depth of 10 mm, the melanin signal can be clearly resolved (see also insets in Fig. 2e). We can fit the data to obtain a characteristic exponential decay in agreement with the radiative transfer equation $I_{PA} = k \exp(-\mu_e d)$. 31,32

As we envisage in vivo imaging applications for linear melanin, we investigate its cell toxicity using in vitro cell culture experiments. Mouse fibroblasts (L929) are incubated with linear melanin at concentrations of up to 10 mM in cell growth media. For all concentrations, the cell morphology is indistinguishable from the control samples without melanin after incubation for 48 h, with nearly 100% life cells. Cells exposed to melanin exhibit brown coloration with melanin being sequestered as small granules in the cytoplasm (see ESI,† Fig. S3). Interestingly, at concentrations of 0.1 mM, a slightly reduced proliferation rate is observed, while concentrations equal or above 1 mM result in almost no proliferation.

In conclusion we have developed a synthetic pathway towards linear melanin with emission in the NIR spectrum and high performance as a contrast agent for photoacoustic imaging and tomography. We can envision further applications of melanin in the diagnostic and theranostic fields. Copolymerization with functional monomers not prone to oxidation would allow for subsequent functionalization with biological recognition motifs, such as antibodies or peptides, or with drugs, rendering our linear and water-soluble melanin a carrier material with intrinsic imaging abilities (e.g. for intravenous drug targeting to tumors). Water-soluble polydopamine and melanin will have a wide spectrum of applications beyond the biomedical fields, for example as electro-active materials in organic electronics or as pigments and radical scavengers in cosmetics.

The authors wish to acknowledge support via the European Research Council (grant no. StG 30 94 95, NeoNaNo) and the excellence initiative of the German federal and state governments and the Hans Hermann Voss-Stiftung through an ERS (Exploratory Research Space @ RWTH Aachen) Seedfund project. The authors thank FujiFilm VisualSonics Inc. for support. This work was performed in part at the Center for Chemical Polymer Technology CPT, which is supported by the EU and the federal state of North Rhine-Westphalia (grant no. EFRE 30 00 883 02).

Notes and references

- 1 Y. Liu, K. Ai and L. Lu, Chem. Rev., 2014, 114, 5057-5115.
- 2 J. Yang, M. A. C. Stuart and M. Kamperman, Chem. Soc. Rev., 2014, 43, 8271-8298
- 3 B.-K. An, X. Wang, P. L. Burn and P. Meredith, ChemPhysChem, 2010, 11, 3517-3521.
- 4 H. Lee, J. Rho and P. B. Messersmith, Adv. Mater., 2009, 21, 431-434.
- 5 L. Hong and J. Simon, J. Phys. Chem. B, 2007, 111, 7938-7947.
- 6 J. D. Simon and D. N. Peles, Acc. Chem. Res., 2010, 43, 1452-1460.
- 7 M. D'Ischia, A. Napolitano, A. Pezzella, P. Meredith and T. Sarna, Angew. Chem., Int. Ed., 2009, 48, 3914-3921.
- 8 Y. Gauslaa and K. Solhaug, Oecologia, 2001, 126, 462-471.
- 9 R. Hoffman, J. Drug Targeting, 1998, 67-74.
- 10 F. P. Noonan, M. R. Zaidi, A. Wolnicka-Glubisz, M. R. Anver, J. Bahn, A. Wielgus, J. Cadet, T. Douki, S. Mouret, M. A. Tucker, A. Popratiloff, G. Merlino and E. C. De Fabo, Nat. Commun., 2012, 3.
- 11 S. E. Forest and J. D. Simon, *Photochem. Photobiol.*, 1998, **68**, 296–298. 12 M. E. Lynge, R. van der Westen, A. Postma and B. Städler, Nanoscale,
- 2011, 3, 4916-4928.
- 13 P. A. Riley, Int. J. Biochem. Cell Biol., 1997, 29, 1235-1239.
- 14 M. Brenner and V. J. Hearing, Photochem. Photobiol., 2008, 84, 539-549.
- 15 H. Lee, S. M. Dellatore, W. M. Miller and P. B. Messersmith, Science, 2007, 318, 426-430.
- 16 S. Hong, Y. S. Na, S. Choi, I. T. Song, W. Y. Kim and H. Lee, Adv. Funct. Mater., 2012, 22, 4711-4717.
- 17 D. R. Dreyer, D. J. Miller, B. D. Freeman, D. R. Paul and C. W. Bielawski, Langmuir, 2012, 28, 6428-6435.
- 18 J. Liebscher, R. Mrówczyński, H. A. Scheidt, C. Filip, N. D. Hădade, R. Turcu, A. Bende and S. Beck, Langmuir, 2013, 29, 10539-10548.
- 19 K.-Y. Ju, Y. Lee, S. Lee, S. B. Park and J.-K. Lee, Biomacromolecules, 2011, 12, 625-632.
- 20 Y. Ding, L.-T. Weng, M. Yang, Z. Yang, X. Lu, N. Huang and Y. Leng, Langmuir, 2014, 30, 12258-12269.
- 21 A. Kumar, S. Kumar, W. Rhim, G. Kim and J. Nam, J. Am. Chem. Soc., 2014, 136, 16317-16325.
- K. Pu, A. J. Shuhendler, J. V. Jokerst, J. Mei, S. S. Gambhir, Z. Bao and J. Rao, Nat. Nanotechnol., 2014, 9, 233-239.
- 23 J. Borovanský and M. Elleder, Pigm. Cell Res., 2003, 16, 280-286.
- 24 J. P. Luther and H. Lipke, *Appl. Environ. Microbiol.*, 1980, **40**, 145–155.
- 25 T. Mammone, K. Marenus, N. Muizzuddin and D. Neelam, J. Cosmet. Sci., 2004, 55, 116-117.
- 26 A. Kiriy, V. Senkovskyy and M. Sommer, Macromol. Rapid Commun., 2011, 32, 1503-1517.
- B. Xiong, Y. Chen, Y. Shu, B. Shen, H. N. Chan, Y. Chen, J. Zhou and H. Wu, Chem. Commun., 2014, 50, 13578-13580.
- 28 E. Faurea, C. Falentin-Daudréa, C. Jérômea, J. Lyskawab, D. Fournier, P. Woisel and C. Detrembleura, Prog. Polym. Sci., 2013, 38, 236-270.
- 29 M. L. Tran, B. J. Powell and P. Meredith, Biophys. J., 2006, 90, 743-752.
- 30 W. Li and X. Chen, Nanomedicine, 2015, 10, 299-320.
- 31 B. Cox, J. G. Laufer, S. R. Arridge and P. C. Beard, J. Biomed. Opt., 2012, 17, 061202.
- 32 G. Marquez, L. V. Wang, S.-P. Lin, J. A. Schwartz and S. L. Thomsen, Appl. Opt., 1998, 37, 798-804.